Alexandria Engineering Journal (2020) 59, 4851–4864

HOSTED BY

Alexandria University

Alexandria Engineering Journal

www.elsevier.com/locate/aej
www.sciencedirect.com

Numerical exploration of MHD falkner-skan-sutterby nanofluid flow by utilizing an advanced non-homogeneous two-phase nanofluid model and non-fourier heat-flux theory

Umair Khan [a], Anum Shafiq [b], A. Zaib [c,d,*], Abderrahim Wakif [e], Dumitru Baleanu [f,g,h]

[a] *Department of Mathematics and Social Sciences, Sukkur IBA University, Sukkur 65200, Sindh, Pakistan*
[b] *School of Mathematics and Statistics, Nanjing University of Information Science and Technology, Nanjing 210044, China*
[c] *Department of Natural Sciences, The Begum Nusrat Bhutto Women University, Sukkur 65170, Pakistan*
[d] *Department of Mathematical Sciences, Federal Urdu University of Arts, Science & Technology, Gulshan-e-Iqbal Karachi 75300, Pakistan*
[e] *Laboratory of Mechanics, Faculty of Sciences Aïn Chock, University Hassan II of Casablanca, Casablanca 20000, Morocco*
[f] *Department of Mathematics, Cankaya University, 06790 Ankara, Turkey*
[g] *Institute of Space Sciences, 077125 Magurele, Romania*
[h] *Department of Medical Research, China Medical University Hospital, China Medical University, Taichung 40447, Taiwan*

Received 15 June 2020; revised 23 August 2020; accepted 28 August 2020
Available online 10 September 2020

KEYWORDS

Sutterby nanofluid;
Magnetohydrodynamics;
Thermophoresis phenomenon;
non-Fourier heat flux

Abstract In this study, the feature of stagnant Sutterby nanofluid towards a wedge surface is analyzed under the impact of a variable external magnetic field. Instead of the traditional Fourier law, the realistic Cattaneo-Christov principle is incorporated in the energy equation to scrutinize the heat flow pattern by utilizing the non-homogeneous two-phase nanofluid model. The constitutive flow rules are transfigured into a nonlinear differential system via feasible mathematical alterations. Methodologically, the bvp4c numerical procedure is employed properly to derive accurate numerical solutions for the present boundary flow problem. By varying the values of the involved parameters of the governing equations, the behaviors of temperature, velocity, and concentration profiles are described graphically and interpreted thoroughly. In this attempt, the major finding is that the magnetic field accelerates the motion and declines the temperature and concentration fields in the performance of suction and injection. Moreover, the nanofluid parameters upsurge the heat transfer mechanism and decline the mass transport and the effect of drag forces in both situations of wall-through flow (i.e., suction and injection effects). Furthermore, the nanofluid concentration profile decays due to the strengthening in the thermophoresis phenomenon. As a useful application, the

* Corresponding author at: Department of Natural Sciences, The Begum Nusrat Bhutto Women University, Sukkur 65170, Pakistan.
E-mail address: aurangzaib@fuuast.edu.pk (A. Zaib).

Peer review under responsibility of Faculty of Engineering, Alexandria University.

https://doi.org/10.1016/j.aej.2020.08.048

Nomenclature

A_1	First tensor of Rivlin Erickson
Λ'	Second invariant tensor
C_1	Concentration
C_w	Wall concentration
C_∞	Ambient concentration
D_B	Brownian diffusion coefficient
D_T	Thermopheritic diffusion coefficient
E	Dimensionless thermal coefficient
K_T	Dimensionless coefficient
M	Magnetic parameter
m	Hartree parameter
n	Material constant
Nb	Brownian motion parameter
Nt	Thermophoretic parameter
Pr	Prandtl number
q_w	Wall Heat flux
q_m	Wall Mass flux
T_1	Dimensional temperature
T_w	Wall temperature
T_∞	Ambient temperature
S	Suction parameter
Sc	Schmidt number
U	Physical constant
V_T	Thermophoresis velocity
v_w	Variable wall suction
v_1, u_1	Velocity components
$u_e(x_1)$	Free-stream or ambient velocity
x_1, y_1	Cartesian coordinates

Greek Symbols

Λ_1	Thermal relaxation time
α	Thermal diffusivity
α_1	Non-Newtonian nanofluid parameter
β_1'	Material constant
δ	Pressure gradient
γ	Thermal relaxation
γ'	Shear stress
μ_0'	Absolute viscosity
ν	Kinematic viscosity
σ'	Electrical conductivity
ρ	Nanofluid density
Re_{x_1}	Reynolds number
τ	Thermophoresis parameter
τ_w	Surface shear stress

Superscript

‘	Derivate w.r.t.η

magnetic function trend along with the thermophoresis diffusion on the nanofluid flow field may be exerted broadly in the field of aerosol technology.

1. Introduction

The phenomenon of heat transport plays a significant role in several geographical mechanisms, industrial and engineering domains. Specific kinds of such mechanisms include tissue heat conduction, electronic device cooling, space cooling, nuclear reactor refrigeration, etc. Because of varying temperatures, heat is transferred inside a body or between two bodies. Heat transport is examined via the Fourier's law of heat conduction over past centuries. Fourier's conventional rule is a curved (parabolic form) equation which demonstrates heat being transferred through unbounded velocity. This rule is called the paradox of transportation. In order to fix this issue, the non-Fourier theory was presented by Cattaneo [1]. He introduced time relaxation factor to Fourier's conventional law so that heat transfers normally by limited velocity. Later on, Christov [2] modified Cattaneo's concept for material-invariant by utilizing the upper-convected Oldroyd's model. Many researchers use this model. Reddy et al. [3] elucidated the cross diffusive properties on MHD flow towards a sheet and cone wedge via the non-Fourier concept. The third-grade nanofluidic flow features towards a Riga surface via the Cattaneo-Christov theory is described by Naseem et al. [4]. Shafiq et al. [5] exposed the significance of the non-Fourier theory on third-grade squeezed the liquid flow among two disks.

The engineers and researchers have been attracted by the novel investigation of flow via the stagnant region. Examples of such flow are flow occurrence among the edges of submarines, oil ships, rockets, and aircraft. Moreover, here two different stagnation point flow (SPF) categories termed orthogonal and oblique. The flow may arise as inviscid, steady, and in several other forms within the stagnation point region. At this point of view, Hiemenz [6] introduced the stagnant point stream analysis and established its exact solution. Mahapatra and Gupta [7], scrutinized the flows about a stagnant point along the stretchable surface by using heat phenomena. Haq et al. [8] stated slip SPF of MHD nanoparticles via radiative stretchable surface. The SPF of Walters' B liquid induced by radiative expanding Riga surface was demonstrated by Shafiq et al. [9]. Khan et al. [10] studied the importance of mixed convective flow (MCF) on a hybrid (SiO_2–MoS_2/H_2O) nanoliquid with the thermal radiation phenomenon via a stagnation point flow. Mabood et al. [11] studied the second-grade stagnant point fluid flow towards a porous non-horizontal stretched cylinder via heat transfer. The magneto-nanoparticles flow of fluid which is (non-Newtonian) deformed through the stretched phenomenon in the stagnant point region was considered by Tian et al. [12]. Mishra et al. [13] scrutinized the impact of heat source on the free convective flow of a non-Newtonian fluid from a shrinking surface. Ismail et al. [14]

analyzed dissipative impacts in a stagnant-point flow along a shrinking surface. Soomro et al. [15] examined the stagnation-point flow involving nanofluid through a moving sheet with nonlinear radiation and heat generation/absorption. Ijaz Khan et al. [16] investigated chemically a reactive CNTs flow in the stagnation point region. Shafiq et al. [17] conducted an analytical investigation on the importance of SPF of a Williamson fluid under the melting phenomenon. Wakif [18] tackled numerically a steady MHD convective non-Newtonina flow probelem over a horizontal irregular stretching sheet by assuming temperature-dependent propreties and considering the preence of thermal radiation.

A novel numerical procedure for simulating steady MHD convective flows of radiative Casson fluids over a horizontal stretching sheet with irregular geometry under the combined influence of temperature-dependent viscosity and thermal conductivity

The aspect of thermophoresis causes tiny materials that are obsessed away from a warm sheet to a cold surface. The tiny materials like dust with temperature gradient while scattering in a gas, occurrence a force in a contrary way to the field of temperature. This aspect has several applications in eradicating tiny materials through gas streams; in shaping drain the trajectories of the gas element from burning devices, and in exploring the particulate substance acknowledgment on blades turbine. In several industries, the symphony of dispensation gases may hold any of an indefinite particle range, fluid, or gaseous impurities and can be prejudiced through unrestrained factors of humidity and temperature. Epstein et al. [19] investigated the free convective flow through a vertical surface with the deposition of thermophoretic particles. Goren [20] focused on the configuration of the horizontal surface in the existence of thermophoresis. The transport of thermophoretic tiny particles in the natural convective flow from a vertical cold surface with erratic flow properties was conferred by Jayaraj et al. [21]. Selim et al. [22] examined the thermophoresis on MCF from a vertical heated flat porous plate with the surface of mass-flux. Wang [23] scrutinized the combined impacts of thermophoresis, diffusion, and inertia through a stagnation-point from a wavy surface. The free MCF in the occurrence of deposition of the thermophoretic of particles through a flat vertical plate immersed in a porous media was Chamkha and Pop [24]. Postelnicu [25] dealt with the impact of thermophoresis on the free convective through a flat horizontal solid surface saturated in the porous medium. The influences of thermophoresis and chemical reaction on MHD flow of nanofluid immersed in a non-Darcy permeable source via a wedge with mixed convection and erratic stream-condition were explored clearly by Muhaimin et al. [26]. A comprehensive *meta*-analysis on the important role of the haphazard motion and thermomigration of tiny particles in the enhancement of the heat and mass transport characteristics of non-homogeneous media were reported recently by Animasaun and his co-worker Wakif in [27,28]. Zaib and Shafie [29] examined the time-dependent MHD flow from a shrinking surface with microrotation and thermophoresis. Recently, Jain and Choudhary [30] discussed the Soret and Dufour numbers of impacts on magneto flow through a nonlinear stretched surface with thermophoresis and chemical reaction.

Nanofluid technology plays a vital role in natural phenomena and industrial processes in several fields involving public health, chemical engineering, physics, biology, and chemistry. Nanofluids are scattered in liquids during processing, handling, production, and undesirable and/or unintentional discharge to the environment. The tiny size of nanomaterials composes it probably to balance their properties of transport to the liquid itself. The Brownian diffusion of particles is one of the significant leading mechanisms to rates of the transport. Physically, Buongiorno [31] elucidated the enhancement of irregular convective heat transport seen in nanofluids. Kuznetsov and Nield [32] scrutinized the natural convective flow involving nanofluid through a vertical surface and discussed the importance of Brownian motion and thermophoretic parameters. Uddin et al. [33] investigated the slip flow for nanoliquid flow comprising bio-convection. By adopting the generalized Buongiorno's nanofluid model, Wakif et al. [34] scrutinized the thermo-magneto-hydrodynamic stability of alumina-copper oxide hybrid nanofluids by including the surface roughness and thermal radiation effects. Similarly, Zaydan et al. [35] utilized the classical non-homogenous nanofluid model to examine the significance of suction and blowing impacts on the occurrence of convective flow in confined nanofluidic media surrounded by a uniform magnetic field. Afterward, several explorations are presented to examine the enhancement of heat transport rate of heat characteristics in the flow field comprising nanofluids through different geometries, such as Rashidi et al. [36], Sheikholeslami et al. [37], Khan et al. [38] and Zahid et al. [39]. Ramezanizadeh and Alhuyi Nazari [40] applied the artificial neural network and correlation to examine the thermal conductivity of water-based silver nanoparticles. Besthapu et al. [41] investigated the impacts of radiation and MHD on the slip flow of a Casson nanofluid from a nonlinear heated stretched sheet. The rotatory Casson nanofluid through a rigid disk with a magnetic force was examined by Rehman et al. [42]. Aman and Al-Mdallal [43] applied the fractional derivative to investigate the Sodium Alginate with Cu nanoparticle and second-order slip. The influence of an erratic heat sink/source on the 3D flow involving Fe_3O_4/Al_2O_3 nanomaterials through a Riga surface with distinct base liquid was explored by Ragupathi et al. [44]. Khan et al. [45] inspected the zero flux condition on the significant impacts of MHD flow of a non-Newtonian nanofluid driven by a stretched/shrinking surface. Ghalandari et al. [46] discussed the nanofluid applications regarding solar energy by employing carbon nanotubes. Recently, Saranya and Al-Mdallal [47] discussed the time-dependent flow of Casson ferrofluid through a contracting cylinder with an externally applied magnetic field. They discussed three kinds of ferroparticles namely, Manganese–Zinc, Cobalt ferrite, and Nickel–Zinc ferrite.

In physiological and industrial processes, the non-Newtonian liquids are more recognized than viscous fluids. Nature contains a diversity of non-Newtonian fluids. Generally, there is no unified constitutive rheological relation that can classify all non-Newtonian liquids according to their diverse characteristics (e.g., shear thinning, shear thickening, viscoelasticity, viscoplasticity, pseudoelasticity, and so on). Therefore, several constitutive rheological models of non-Newtonian liquids were proposed. Among those, the Sutterby rheological model is one that describes the aqueous solutions exhibiting a higher level of polymer concentration. So far, many scientists have paid enormous attention to the Sutterby fluid flows. Despite this concern, the motion of Sutterby nanofluids still has not been discussed yet by the researchers for the non-Newtonian flows over a wedge surface. The main

effort here is to venture further in this topic by adopting the non-Fourier heat flux along with the Brownian motion and thermophoresis aspects to study the suction and injection impacts on MHD stagnation point flow of Sutterby nanofluid over the permeable surface of a static wedge. To the best of the author's knowledge, no such analysis has been presented before. For this purpose, an enhanced non-homogeneous two-phase nanofluid model has been proposed in this investigation to simulate numerically a steady MHD Falkner-Skan convective flow for Sutterby nanofluids in the sense of Cattaneo-Christov heat flux theory. Based on strong theoretical frameworks and assumptions, the system of conservation equations was established properly along with their appropriate hydrodynamic, thermal, and concentration boundary conditions. After some simplifying transformations, the resulting nonlinear differential system was solved numerically by utilizing the bvp4c numerical procedure. It is important to noting that the Generalized Differential Quadrature Method (GDQM) [48–53], the Chebyshev-Gauss-Lobatto spectral method (CGLSM) [54–56], as well as the Spectral Element Method (SEM) [57–61] can be also exploited as powerful techniques to solve the governing nonlinear differential equations of the present flow model. Finally, the obtained findings (i.e., velocity, temperature, concentration, as well as heat and mass transport rates) are discussed thoroughly and elucidated physically via various graphical and tabular demonstrations showing the interesting features of the present non-Newtonian boundary flow problem.

2. Physical description and modeling

A 2D steady MHD boundary layer flow involving a Sutterby nanofluid over the permeable surface of a static wedge is presented through the non-Fourier heat flux theory. The erratic magnetic field of strength B is applied perpendicularly to the wedge surface as shown in Fig. 1.

According to Patil et al. [62] and Hayat et al. [63], the Sutterby rheological stress tensor is defined as

$$S_1 = \frac{\mu_0'}{2}\left[\frac{\sinh^{-1}(\beta_1'\gamma')}{\beta_1'\gamma'}\right]^n A_1, \tag{1}$$

where

$$A_1 = (\text{grad V}) + (\text{grad V})^T, \tag{2}$$

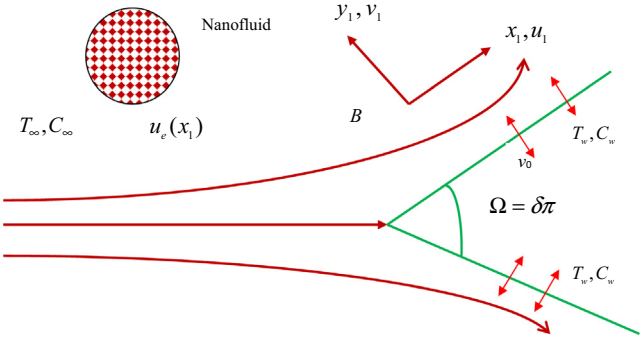

Fig. 1 Geometry of the problem.

$$\gamma' = \left(\sum_i \sum_j \gamma_{1i}'\gamma_{j1}'\right)^{\frac{1}{2}} = \left(\frac{\Lambda'}{2}\right)^{\frac{1}{2}}, \tag{3}$$

$$\Lambda' = \text{trace}[(\text{grad V}) + (\text{grad V})^T]^2. \tag{4}$$

In the above expressions, n and β_1', γ', μ_0', A_1 and Λ', respectively signify the materials constants, the shear stress, the absolute viscosity, the first tensor of Rivlin Erickson and the second invariant tensor.

For $\beta_1'\gamma' << 1$, we have

$$\sinh^{-1}(\beta_1'\gamma') \cong \beta_1'\gamma' - \frac{(\beta_1'\gamma')^3}{6}, \tag{5}$$

The relation of viscosity for the Sutterby liquid is

$$\mu = \mu_0'\left[\frac{\sinh^{-1}(\beta_1'\gamma')}{\beta_1'\gamma'}\right]^n \cong \mu_0'\left[1 - \frac{(\beta_1'\gamma')^2}{6}\right]^n. \tag{6}$$

The leading relevant PDEs by applying boundary-layer assumptions are [62–65]

$$\frac{\partial u_1}{\partial x_1} + \frac{\partial v_1}{\partial y_1} = 0, \tag{7}$$

$$u_1\frac{\partial u_1}{\partial x_1} + v_1\frac{\partial u_1}{\partial y_1} = \nu\left(1 - \frac{\beta_1'^2}{6}\frac{\partial u_1}{\partial y_1}\right)^n \frac{\partial^2 u_1}{\partial y_1^2} - \frac{n\nu\beta_1'^2}{6}\left(1 - \frac{\beta_1'^2}{6}\frac{\partial u_1}{\partial y_1}\right)^{n-1}\frac{\partial u_1}{\partial y_1}\frac{\partial^2 u_1}{\partial y_1^2} + u_e \times \frac{du_e}{dx_1} - \frac{\sigma' B^2}{\rho}(u_1 - u_e), \tag{8}$$

$$u_1\frac{\partial T_1}{\partial x_1} + v_1\frac{\partial T_1}{\partial y_1} = \left\{\alpha\frac{\partial^2 T_1}{\partial y_1^2} + \text{E}\left[D_B\left(\frac{\partial T_1}{\partial y_1}\frac{\partial C_1}{\partial y_1}\right) + \frac{D_T}{T_\infty}\left(\frac{\partial T_1}{\partial y_1}\right)^2\right] + \Lambda_1\left[u_1\frac{\partial u_1}{\partial x_1}\frac{\partial T_1}{\partial x_1} + v_1\frac{\partial v_1}{\partial y_1}\frac{\partial T_1}{\partial y_1} + u_1\frac{\partial v_1}{\partial x_1}\frac{\partial T_1}{\partial y_1} + v_1\frac{\partial u_1}{\partial y_1}\frac{\partial T_1}{\partial x_1} + 2u_1v_1\frac{\partial^2 T_1}{\partial x_1\partial y_1} + u_1^2\frac{\partial^2 T_1}{\partial x_1^2} + v_1^2\frac{\partial^2 T_1}{\partial y_1^2}\right]\right\}, \tag{9}$$

$$u_1\frac{\partial C_1}{\partial x_1} + v_1\frac{\partial C_1}{\partial y_1} = D_B\frac{\partial^2 C_1}{\partial y_1^2} + \frac{D_T}{T_\infty}\left(\frac{\partial^2 T_1}{\partial y_1^2}\right) - \frac{\partial((C_1 - C_\infty)V_T)}{\partial y_1}. \tag{10}$$

with the boundary conditions

$$\begin{aligned} &u_1 = 0,\ v_1 = v_w(x_1) = -v_0 x_1^{\left(\frac{m-1}{2}\right)}\left(\frac{Uv(1+m)}{2}\right)^{-\frac{1}{2}},\\ &T_1 = T_w,\ C_1 = C_w \text{ at } y_1 = 0,\\ &u_1 \to u_e = Ux_1^m,\ T_1 \to T_\infty,\ C_1 \to C_\infty \text{ as } y_1 \to \infty. \end{aligned} \tag{11}$$

As shown above, the physical quantities C_1, T_1, ν, σ', ρ and α signify the concentration, the temperature, the kinematic viscosity, the electrical conductivity, the density, and the thermal diffusivity, respectively. (v_1, u_1) denote the components of nanofluid velocity in the (y_1, x_1) directions, respectively, Λ_1 marks the thermal relaxation time, T_w and C_w designate the

wall temperature and concentration, $u_e(x_1)$ represents the free-stream or ambient velocity, C_∞ and T_∞ show the ambient concentration and temperature, v_w highlights the variable wall suction, U symbolizes a physical constant, δ stands for the pressure gradient Hartree parameter,m characterizes a power index appeared in the expression of the suction velocity v_w, where $m = \delta/(2-\delta)$ and $\delta = \Omega/\pi$, D_T elucidates the thermal diffusion, D_B describes the Brownian diffusion, E defines a dimensionless thermal factor, and $V_T = (vK_T/T_r)(\partial T_1/\partial y_1)$ gives the analytical expression of the thermophoresis velocity V_T. Here, the thermal quantity T_r corresponds to a reference temperature and K_T indicates a dimensionless coefficient

Further, this analysis can be eased by utilizing the following similarity variables as

$$\left\{\begin{array}{l} \eta = y_1\left[\frac{(1+m)U}{2v}\right]^{\frac{1}{2}} x_1^{\left(\frac{m-1}{2}\right)}, \psi = \left(\frac{2Uv}{1+m}\right)^{\frac{1}{2}} \\ x_1^{\left(\frac{m+1}{2}\right)} F(\eta), \theta(\eta) = \frac{T_1 - T_\infty}{T_w - T_\infty}, \\ \chi(\eta) = \frac{C_1 - C_\infty}{C_w - C_\infty}, u_1 = U x_1^m F', \\ v_1 = -\left[\frac{Uv(1+m)}{2}\right]^{\frac{1}{2}} x_1^{\left(\frac{m-1}{2}\right)}\left[F + \left(\frac{m-1}{m+1}\right)\eta F'\right], \\ \beta_1'^2 = \frac{\beta_0^2}{x_1^{m-1}}, B = B_0 x_1^{\left(\frac{m-1}{2}\right)}, \Lambda_1 = \frac{\Lambda_2}{x_1^{m-1}}. \end{array}\right\} \tag{12}$$

Publicizing the transformations in the leading PDEs, one gets the ODEs in the following dimensional form

$$\left[1 - \frac{\alpha_1}{6}\left(\frac{m+1}{2}\right)^{\frac{1}{2}} F''\right]^n F''' - \frac{n\alpha_1}{6}\left(\frac{m+1}{2}\right)^{\frac{1}{2}}\left[1 - \frac{\alpha_1}{6}\left(\frac{m+1}{2}\right)^{\frac{1}{2}} F''\right]^{(n-1)} F''F''' - \frac{2m}{m+1}\left(F'^2 - 1\right) + FF'' - \frac{2M}{m+1}(F' - 1) = 0, \tag{13}$$

$$\theta'' + \Pr\left[F\theta' - \gamma\left(\left(\frac{m-3}{2}\right)FF'\theta' - \left(\frac{m+1}{2}\right)F^2\theta''\right)\right] + \theta'(\chi' Nb + Nt\theta') = 0, \tag{14}$$

$$\chi'' + ScF\chi' + \frac{Nt}{Nb}\theta'' - \tau Sc(\chi'\theta' + \chi\theta'') = 0, \tag{15}$$

with the boundary conditions

$$F'(\eta) = 0,\ F(\eta) = S,\ \theta(\eta) = 1,\ \chi(\eta) = 1 \text{ at } \eta = 0,\quad F'(\eta) \to 1,\ \theta(\eta) \to 0,\ \chi(\eta) \to 0 \text{ as } \eta \to \infty, \tag{16}$$

where $\alpha_1 = \beta_0^2 U Re_{x_1}^{1/2}$ is the non-Newtonian nanofluid parameter, $Re_{x_1} = u_e x_1/v$ is the Reynolds number, $M = \sigma' B_0^2/\rho U$ is the magnetic number, $\Pr = v/\alpha$ is the Prandtl number, $Nb = ED_B(C_w - C_\infty)/\alpha$ is the Brownian motion, $Nt = ED_T(T_w - T_\infty)/T_\infty\alpha$ is the thermophoretic parameter, $S = 2v_0/Uv(1+m) > 0$ is the suction parameter and $S = 2v_0/Uv(1+m) < 0$ is the injection parameter, $\gamma = \Lambda_2 U$ is the thermal relaxation, $Sc = v/D_B$ is the Schmidt number and $\tau = K_T(T_w - T_\infty)/T_r$ is the thermophoresis parameter.

The expressions of Skin friction factor, Nusselt number, and Sherwood number are given as

$$\left\{\begin{array}{l} C_F = \frac{\tau_w}{\rho u_e^2}, \\ Nu_{x_1} = \frac{x_1 q_w}{k_f(T_w - T_\infty)}, \\ Sh_{x_1} = \frac{x_1 q_m}{D_B(C_w - C_\infty)}. \end{array}\right\} \tag{17}$$

Additionally, the surface shear stress τ_w, the wall heat flux q_w , and the wall mass flux q_m are computed as

$$\left\{\begin{array}{l} \tau_w = \left[1 - \frac{\beta_1'^2}{6}\left(\frac{\partial u_1}{\partial y_1}\right)\right]^n \left(\frac{\partial u_1}{\partial y_1}\right)\Big|_{y_1=0}, \\ q_w = -k_f\left(\frac{\partial T_1}{\partial y_1}\right)\Big|_{y_1=0}, \\ q_m = -D_B\left(\frac{\partial C_1}{\partial y_1}\right)\Big|_{y_1=0}. \end{array}\right\} \tag{18}$$

Then, the dimensional forms of the physical quantities of major interest are

$$\left\{\begin{array}{l} Re_{x_1}^{0.5} C_F = \left(\frac{m+1}{2}\right)^{\frac{1}{2}}\left[1 - \frac{\alpha_1}{6}\left(\frac{m+1}{2}\right)^{\frac{1}{2}} F''(0)\right]^n F''(0), \\ Re_{x_1}^{-0.5} Nu_{x_1} = -\left(\frac{m+1}{2}\right)^{\frac{1}{2}}\theta'(0), \\ Re_{x_1}^{-0.5} Sh_{x_1} = -\left(\frac{m+1}{2}\right)^{\frac{1}{2}}\chi'(0), \\ Re_{x_1} = \frac{U x_1^{(m+1)}}{v}. \end{array}\right\} \tag{19}$$

3. Results and discussion

The simulation of a two-phase model comprising a Sutterby nanofluid flow through a static wedge with the thermophoresis and magnetic field is performed numerically. In order to work out numerically the transmuted ODEs (13)-(15) with restrictions (16), a bvp4c is utilized. The effects of the non-Newtonian nanofluid parameter, the magnetic parameter, the wedge parameters, the Brownian motion parameter, the thermophoretic parameter, the thermal relaxation parameter, as well as the thermophoresis mechanism on the studied nanofluid flow are reported clearly with its heat and mass transfer characteristics considering the existence of suction and injection. To authenticate the exactness of the current outcomes, a comparison is made with the established solutions of Yih [66] and Yacob et al. [67] in a specified limiting case. This assessment depicts an outstanding harmony as shown in Table 1.

3.1. Effect of the magnetic parameter (M)

Figs. 2–4 explore the effect of the magnetic factor on the velocity, temperature, and concentration profiles, respectively. These figures are individually plotted and show the variations for suction which is represented by the solid green lines and consequently the dashed red lines show the variations for the injection. Fig. 2 shows that the velocity has been detected to amplify for both the suction (SUC) and injection (INJ). The velocity behavior is augmented in both phenomena of SUC and INJ as we upsurge the impact of the magnetic parameter. This fact is explained by the negative sign of the Lorentzian

Table 1 Comparison of the numerical values of $F''(0)$ for distinct m when $\alpha = M = 0$.

m	Yih [66]	Yacob et al. [67]	Present
0	0.469600	0.4696	0.4696
1/11	0.654979	0.6550	0.6550
0.2	0.802125	0.8021	0.8021
1/3	0.927653	0.9277	0.9277
0.5	———	1.0389	1.0389
1	1.232588	1.2326	1.2326

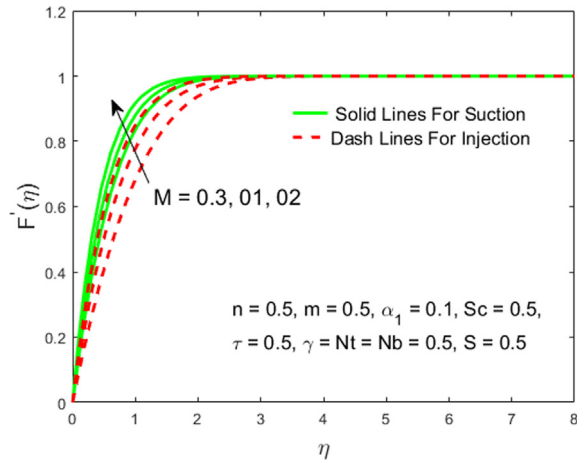

Fig. 2 Influences of M on $F'(\eta)$.

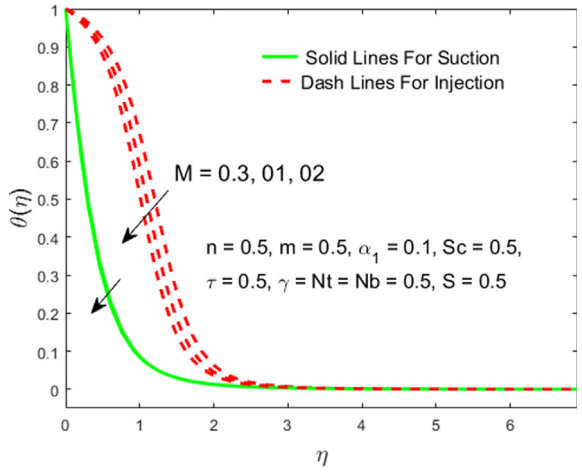

Fig. 3 Influences of M on $\theta(\eta)$.

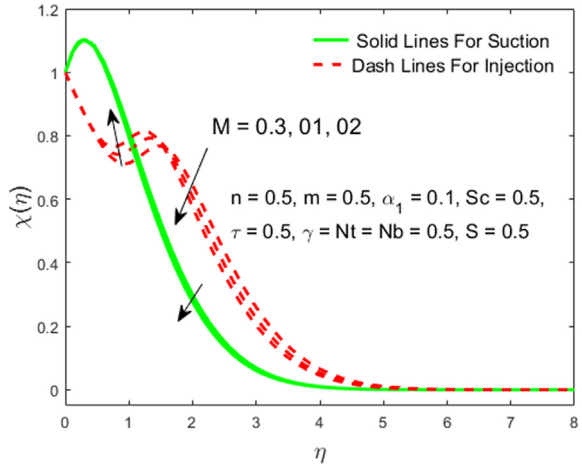

Fig. 4 Influences of M on $\chi(\eta)$.

term $\frac{\sigma' B^2}{\rho}(u_1 - u_e)$ that appears in Eq. (8). For the velocity profile, the impacts are so prominent, but a closer view of the current scenario addresses that the suction effect is more dominant than the injection impact. The behavior of the temperature and concentration profiles are decreasing for the SUC as well as INJ owing to the effect of the higher magnetic parameter are highlighted in Figs. 3 and 4, respectively. Physically, the conception of Lorentz forces via an increment in the magnetic parameter creates a noticeable boost in the flow, which ultimately declines the temperature as well as the concentration due to the colling effect of the free-stream flow. Moreover, it is noteworthy to observe that the deviation of the temperature behavior in each curve is a little bit less for suction as matched to the injection while for the field of concentration the deviation in each curve is distinct in terms of behavior (like temperature distribution) from the case of suction and as well as for injection. Table 2 expresses that the increasing rate of the (M) on the skin factor is 20.70% for the suction, whereas for the injection it is 35.49%.

3.2. *Effect of the wedge parameter* ($\boldsymbol{m}$) *and wedge angle* (Ω)

Figs. 5–7 are portrayed to perceive the influences of either (m) or (Ω) on the velocity, temperature, and concentration profiles for both the suction and injection. Fig. 5 shows that the flow velocity is increasing for the INJ and SUC owing to the larger impact of either (Ω) or (m). Physically, owing to the suction process, the warm nanofluid is depressed towards the surface of the wedge where the forces can progress to augment the nanofluid velocity. Additionally, it is noticed that the deviation in each curve for the injection is a little bit larger as matched with the solutions of SUC. Fig. 6 shows the augmentation in the temperature distribution for the suction due to the higher values of the parameter either (m) or (Ω) while consequently, the temperature behavior depreciated for the injection. More precisely, the variation in each curve for the suction is wider than the injection as we can see the clear, concise behavior in the plot of the temperature profile. The field of concentration is sealed in Fig. 7 where the behavior is deliberately shown a decreasing trend for both the SUC and INJ owing to the boosted values of either (m) or (Ω). The gap in each curve for the suction as well as injection are approximately looking the same in the concentration profile while a very change gap is noticed in the comparison of velocity field and temperature distribution for both suction and injection. From Table 2, it is apparent that for the three distinct values of the parameter either (m) or (Ω)displays that the skin factor is growing with the rate of 6.21% for the suction, while for the injection it boosts up with the concentration rate of 8.02%. On the contrary side, the Nusselt number owing to the percentage-wise, it is increased up to 11.93% in the injection while for the case of suction it is 0.09% which is comparatively very low like the skin friction.

3.3. *Effect of the non-Newtonian nanofluid parameter* (α_1)

Fig. 8 demonstrates the impact of the non-Newtonian nanofluid parameter (α_1) on the field of velocity. The motion of the nanofluid flow is detected inclined for both the suction and injection owing to the elevation in the parameter (α_1). It is reflected from the plot that the momentum boundary layer thickness is more dominant for the SUC as we compared to the INJ. Similarly, the gap between the individual curves is slightly bigger for the suction in the response of injection.

Table 2 The numerical values of the friction factor for distinct values of M, m and α_1 when $n = Sc = \tau = \gamma = Nb = Nt = 0.5, S = 0.01$.

M	m	α_1	Suction	Injection
0.3	0.5	0.3	1.3057	0.8199
1.0			1.5760	1.1109
1.5			1.7402	1.2829
0.3	0.4	0.3	1.2293	0.7590
	0.5		1.3057	0.8199
	0.6		1.3776	0.8767
0.3	0.5	0.1	1.3132	0.8253
		0.5	1.2978	0.8142
		0.9	1.2806	0.8024

The skin friction values for both the phenomenon decelerate for augmenting (α_1) as shown in Fig. 9. From Table 2, it is detected more critically that the reduction rate of the skin factor for the parameter (α_1) is 1.34% for the injection, whereas for the suction it is 1.17%. Physically, as we boost up the value of the factor (α_1), the viscosity of the nanofluid is diminished and as outcomes, the field of skin friction decrements, and the velocity of the field elevates. Furthermore, the impact of the non-Newtonian nanofluid parameter on the Nusselt and the Sherwood number versus the magnetic parameter are highlighted in Figs. 10 and 11, respectively. The Nusselt number elevates for both the suction and as well as for injection owing to the bigger values of the parameter (α_1), while a contrary behavior (like Fig. 10) is observed for the rate of mass transfer. The outcome values of the rate of heat transfer for the suction are bigger than the case of injection and this current scenario is behaviorally sealed in the graph (Fig. 10) while the Sherwood number outcomes are very low for the suction as compared to injection (see Fig. 11). In other words, the gap among the curves for the suction and injection for both Nusselt and Sherwood numbers are slightly the same but behaviorally different.

3.4. *Effect of the Brownian parameter* (***Nb***) *and thermophoretic parameter* (***Nt***)

Figs. 12–15 reveal the influence of the Brownian motion parameter (Nb) and the thermophoresis parameter (Nt) against the similarity variable (η) for the specific numerical values of suction and injection. Fig. 12 depicts the deviation of the parameter Nb on the temperature distribution. The temperature field is an augmenting function for the suction as well as for injection owing to the larger values of Nb. As expanding the phenomenon of Brownian motion which accelerates the process of collision of nanomaterials and particles of liquid moving fast, this collision slaughters the particles' mechanical energy that transmuted into thermal form, and consequently, the nanofluid temperature upsurges. Very similar behavior is noticed (like Fig. 12) for the impact of the thermophoresis parameter on the temperature filed as represented in Fig. 13. As thermophoretic force thrusts the particles of the hot nanofluid far from the wedge surface, this procedure hastens the thermal energy transportation into liquid far from the wedge surface. Consequently, the liquid temperature uplifts very quickly for both the values of suction and injection. Moreover, the gap between the curves is comparatively very small due to the influences of Nb and Nt on the temperature field and we noticed this observation more clearly from the graph, but numerically we can differentiate their differences in the tabular form for suction and injection. From Table 3, the reduction rate of the Nusselt number for the suction is 3.21% and 1.93%, while for the injection it is 6.37% and 10.24% owing to the parameter $Nb$and Nt, respectively. Thus, the rate of reduction due to the parameter Nt is more for the suction as compared to the impact of the parameter Nb while it is opposite for the injection. Fig. 14 describes the impact of the constraint Nb on the concentration field for the SUC as well as for the INJ. The concentration field is a reduced function with the augmentation values of Nb for the positive and negative values of S. In fact, when the Nb grows, the collision between the particles of the nanofluidic medium improves and ensures a lower mass transport phenomenon from the heated sheet towards the cold nanofluidic region. Therefore, the concentration field shows decelerating behavior for both SUC and INJ. Additionally, the concentration profile is more dominant for the suction as compared to the injection owing to the impact of Nb. Fig. 15 portrays that the concentration field behaves totally opposite (like Fig. 14) for the suction and injection as we augmented the values of the parameter Nt. Augmenting behavior of the field of concentration is observed for dominant values of Nt for both suction and injection. Moreover, it is perceived that the boundary layer concentration increases for the larger Nt. The boundary layer of the field of concentration is thinner in injection as compared to suction. Table 4 defines the numerical values for the distinct parameters; here we especially focused on the impact of Nb where the increasing rate of the concentration for the suction is 74.36%, whereas the decreasing rate of the concentration for the injection is 11.93%. On the other hand, the variation of the parameter Nt for the three distinct values numerically explained that the concentration rate is decelerated for the suction by 88.64%, while accelerated with the rate of 17.73% for the injection as shown in Table 4.

3.5. *Effect of the thermal relaxation parameter* (γ)

Figs. 16 and 17 represent the variation of the thermal relaxation parameter on the temperature and concentration fields versus the similarity variable (η), respectively. The nanofluid flow behavior for the field of temperature and concentration is detected in the case of suction as well as in the case of injection. The individual influence of the parameter on the temperature field is revealed in Fig. 16. The thermal boundary layer

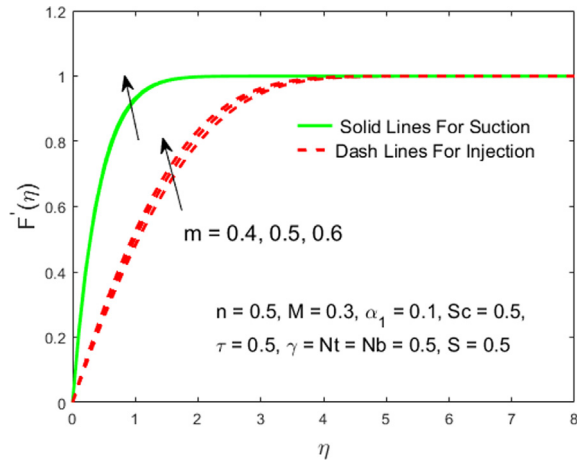

Fig. 5 Influences of m on $F'(\eta)$.

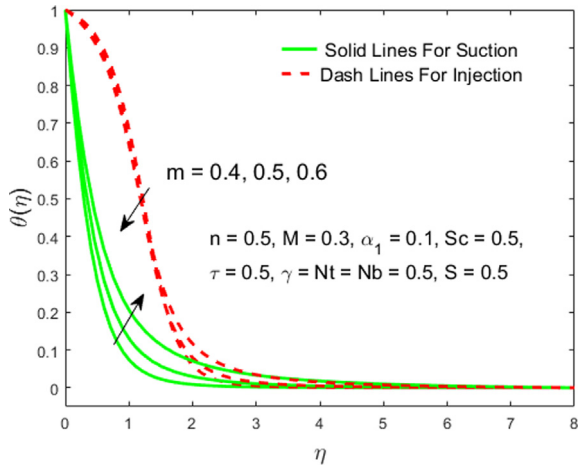

Fig. 6 Influences of m on $\theta(\eta)$.

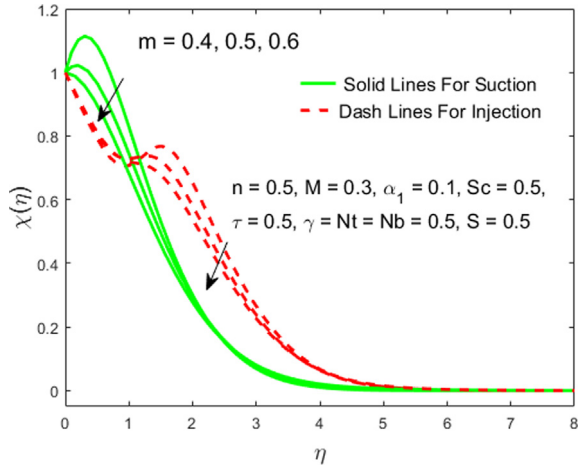

Fig. 7 Influences of m on $\chi(\eta)$.

and its associated flow of the temperature are elevated for the suction and decelerate for the injection as we augmented the value of the parameter γ. Further, it is observed that the gap

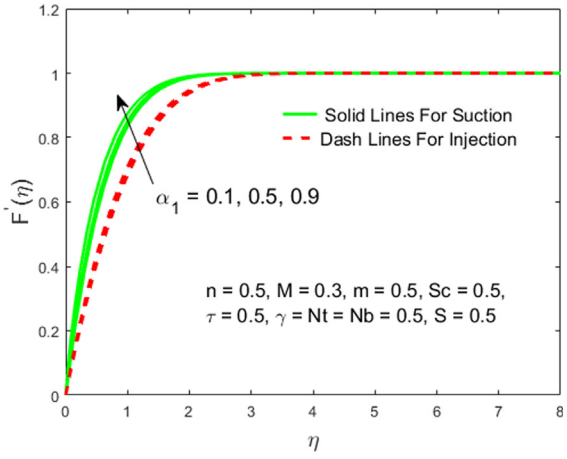

Fig. 8 Influences of α_1 on$F'(\eta)$.

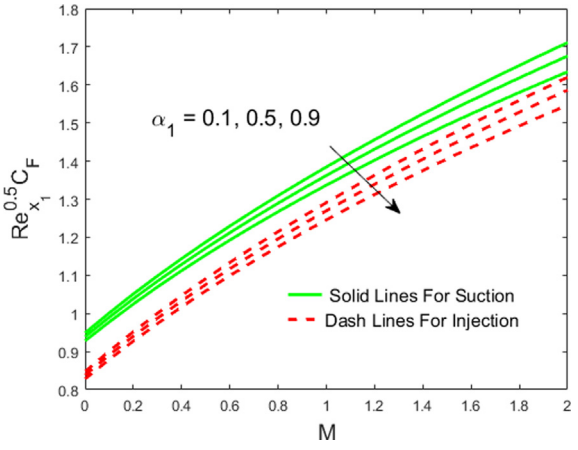

Fig. 9 Deviation of the skin friction versus M for distinct values of α_1.

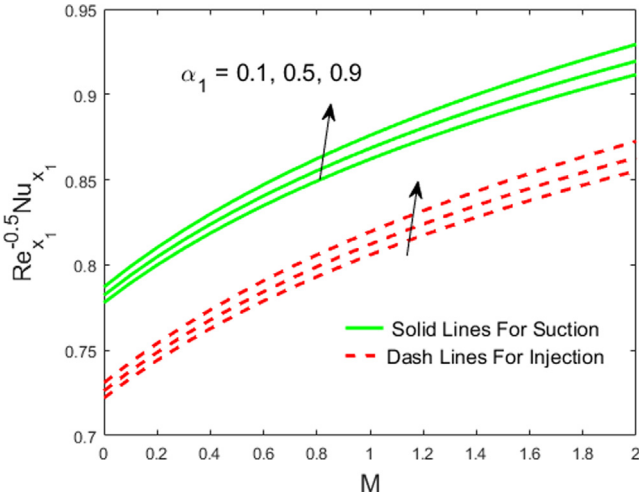

Fig. 10 Deviation of the Nusselt number versus M for distinct values of α_1.

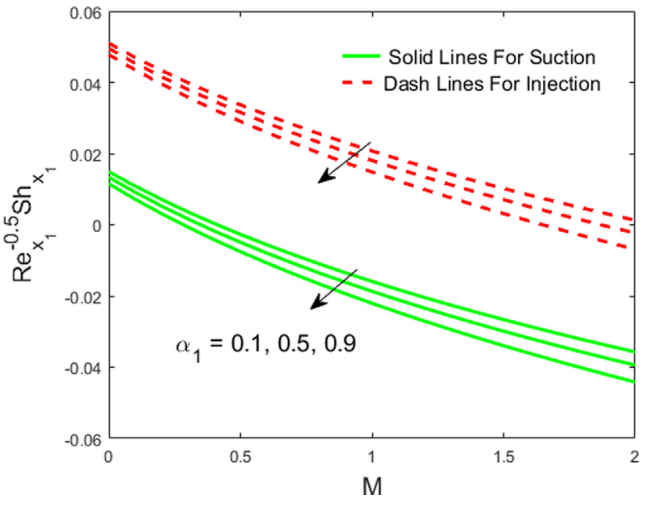

Fig. 11 Deviation of the Sherwood number versus M for distinct values of α_1.

in each of the individual curves for the suction is a little bit more than the injection. More generally, owing to the bigger value of γ, the molecules of the substantial quantity require more time to conduct heat to its adjacent particles, but due to the presence of the stagnation point, it helps and reduces the time to transport heat. Precisely, for higher γ, and influence of the stagnation point the material displays a conducting characteristic for the case of suction which is accountable in the escalating of temperature distribution while in the case of injection the material shows a non-conducting behavior and as a consequence, the temperature field is decaying. The numerical outcomes of the Nusselt number owing to the parameter γ which is defined in Table 3, where the reduction rate is 8.06% for the suction and the increasing rate is 7.89% in the injection. Fig. 17 displays the impact of the parameter γ on the field of concentration. In fact, the concentration field is initially decreased and then increased for the suction in the response of the thermal relaxation parameter while for the injection it is decelerating. Therefore, the field of concentration and its associated concentration boundary

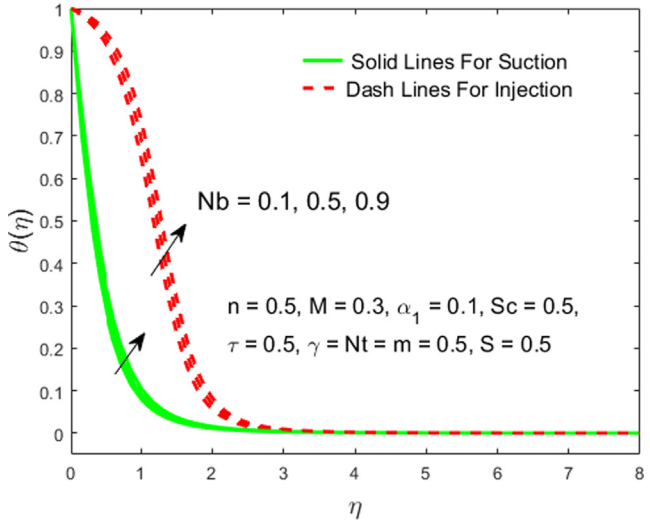

Fig. 12 Influences of Nb on $\theta(\eta)$.

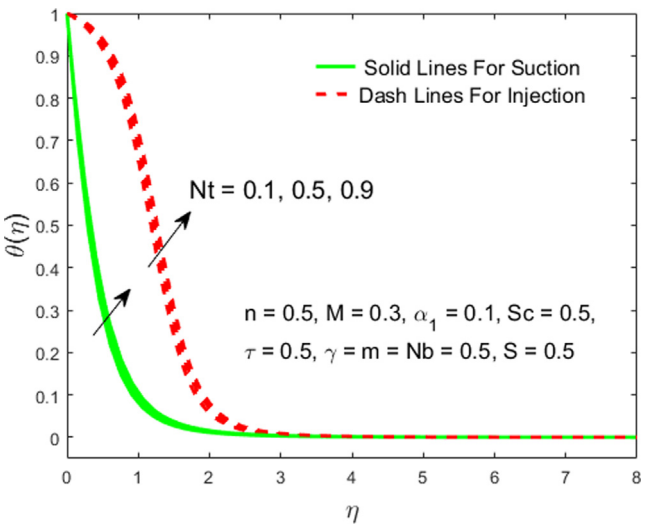

Fig. 13 Influences of Nt on $\theta(\eta)$.

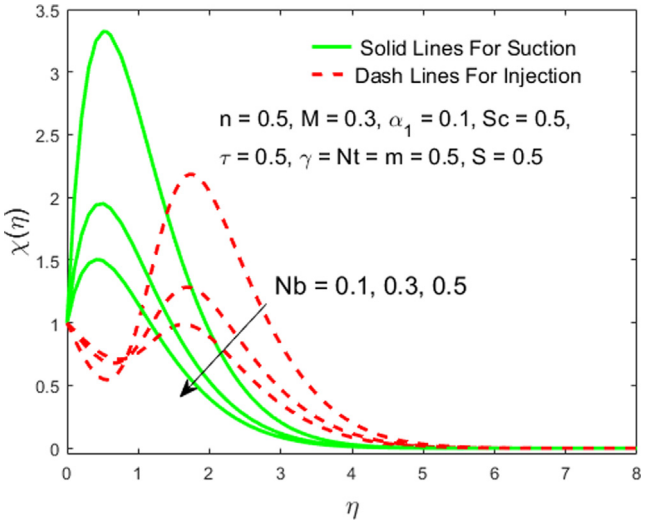

Fig. 14 Influences of Nb on $\chi(\eta)$.

layer is showing an increment for the suction and decrement for the injection.

3.6. Effect of the thermophoresis parameter(τ) *and Schmidt number* (***Sc***)

Figs. 18 and 19 explored the deviation of the parameter (Sc) and (τ) on the field of concentration for both the cases of the mass flux parameter. Fig. 18 shows the concentration lines for the suction as well as for the injection. The concentration field falls off in both cases. Physically, this happens owing to a diminution in the Brownian diffusion coefficient. From Table 4, it is detected that the Sherwood number increases with the rate of 50.21% in the suction while in the injection, it is 3.27%. The impact for the parameter τ on the concentration profile for both the cases is revealed in Fig. 19. It is perceived that the nanofluid concentration declines with the rise of the thermophoresis parameter, whereas the variation in the pro-

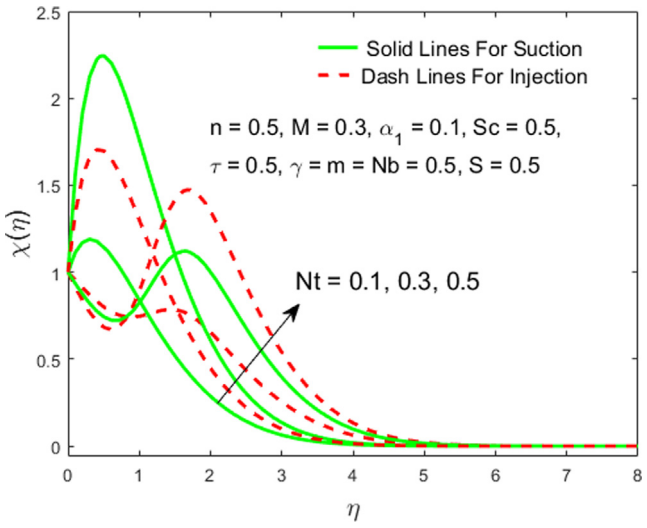

Fig. 15 Influences of Nt on $\chi(\eta)$.

files of velocity and temperature is not significant with the increase in the thermophoresis parameter. Especially, the increase of the parameter τ is restricted to growing vaguely the slope of the wall of the concentration but declining the boundary layer of concentration as well. This fact is true in the case of a small amount of Sc where the Brownian impact is greater compared to the influence of convection. But, for a higher amount of Sc, the effect of diffusion is smallest compared to the effect of convection and thus, thermophoresis impact is estimated to modify significantly the concentration boundary-layer. This work is consistent with the results of Goren [20] on the thermophoresis of aerosol particles within a laminar boundary layer flow on a flat surface. The Sherwood number reduction rate for the thermophoresis parameter in the case of injection is 6.44%, while the increasing rate in the suction is 65.26% as portrayed in Table 4.

3.7. Variation of the Nusselt and Sherwood numbers

Fig. 20 depicts the impact of Nb and Nt on the Nusselt number, while Fig. 21 displays the influence of Nt and τ on the Sherwood number. Fig. 20 explains that the thermophoretic and Brownian motion parameters have declined the Nusselt number. In addition, the change in the rate of heat transfer is detected to be larger for a smaller amount of Nb. Fig. 21 suggests that the Sherwood number augments due to thermophoresis parameter and declines due to Nt. Interesting

Table 3 The numerical values of the Nusselt number for distinct values of γ, m, Nb and Nt when $n = Sc = \tau = 0.5, S = 0.01, M = 0.3, \alpha_1 = 0.3$.

γ	m	Nb	Nt	Suction	Injection
0.5	0.5	0.5	0.5	1.8475	0.0722
0.7				1.6985	0.0779
0.9				1.5857	0.0825
0.5	0.4	0.5	0.5	1.8458	0.0645
	0.5			1.8475	0.0722
	0.6			1.8523	0.0797
0.5	0.5	0.5	0.5	1.8475	0.0722
		0.7		1.7881	0.0676
		0.9		1.7303	0.0633
0.5	0.5	0.5	0.5	1.8475	0.0722
			0.7	1.8117	0.0684
			0.9	1.7766	0.0648

Table 4 The numerical values of the Sherwood number for distinct values of Sc, τ, Nb and Nt when $n = \gamma = m = 0.5, S = 0.01, M = 0.3, \alpha_1 = 0.3$.

Sc	τ	Nb	Nt	Suction	Injection
0.5	0.5	0.5	0.5	−0.6440	0.3880
0.7				−0.3206	0.4007
0.9				−0.0242	0.4009
0.5	0.5	0.5	0.5	−0.6440	0.3880
	01			−0.2237	0.3630
	1.5			0.1829	0.3408
0.5	0.5	0.5	0.5	−0.6440	0.3880
		0.7		−0.1651	0.3417
		0.9		0.0939	0.3157
0.5	0.5	0.5	0.5	−0.6440	0.3880
			0.7	−1.2349	0.4568
			0.9	−1.7986	0.5271

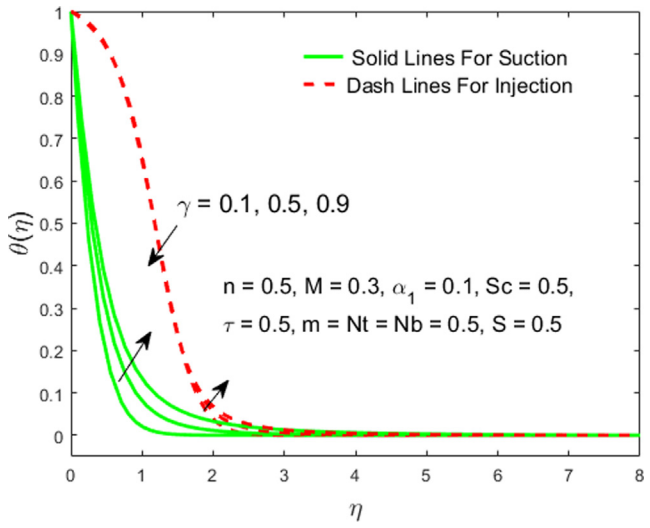

Fig. 16 Influences of γ on $\theta(\eta)$.

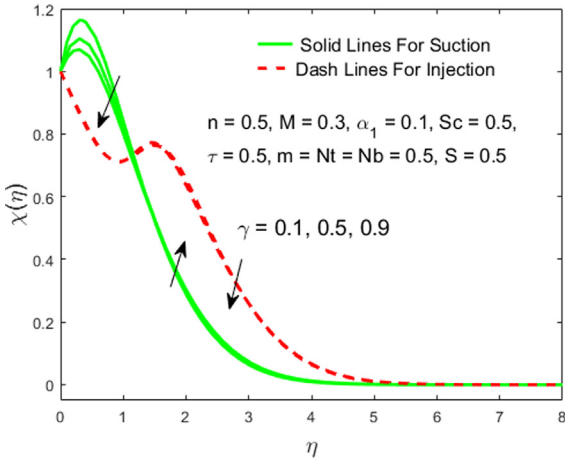

Fig. 17 Influences of γ on $\chi(\eta)$.

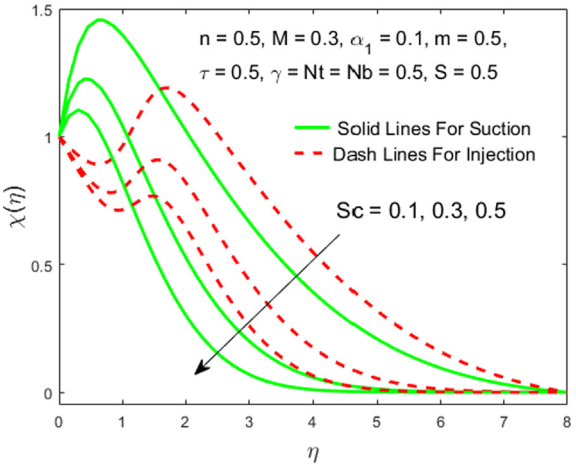

Fig. 18 Influences of Sc on $\chi(\eta)$.

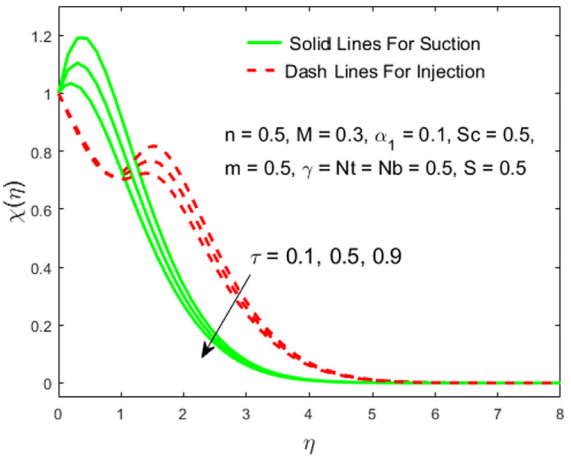

Fig. 19 Influences of τ on $\chi(\eta)$.

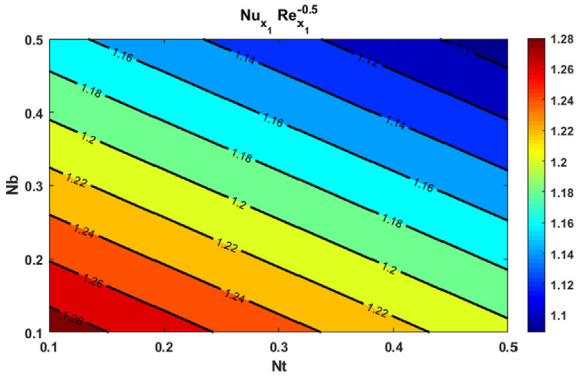

Fig. 20 Influences of Nt and Nb on $Re_{x_1}^{-0.5} Nu_{x_1}$ when $n = 0.5, M = 0.5, \tau = 0.5, \alpha = 0.1, m = 0.5, S = 2$.

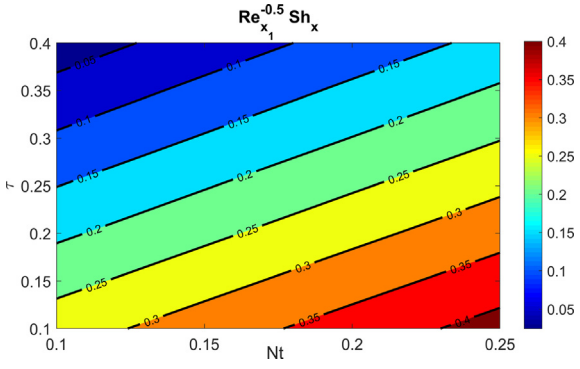

Fig. 21 Influences of Nt and τ on $Re_{x_1}^{-0.5} Sh_{x_1}$ when $n = 0.5, M = 0.5, Nb = 0.5, \alpha = 0.1, m = 0.5, S = 0.1$

behavior on the streamlines can be seen in Figs. 22 and 23 in the existence of suction and injection. The patterns portray that the streamlines are more obscured and split into two regions in the choice of INJ, while in the choice of SUC; the patterns are simple and follow the flow field.

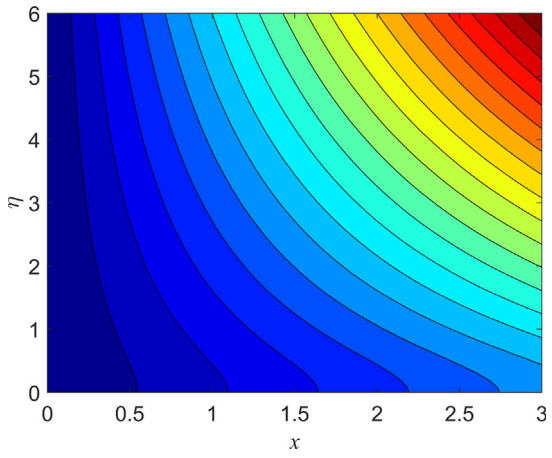

Fig. 22 The patterns of streamlines in the case of suction when $n = 0.5, M = 0.5, \tau = 0.5, \alpha = 0.1, m = 1$.

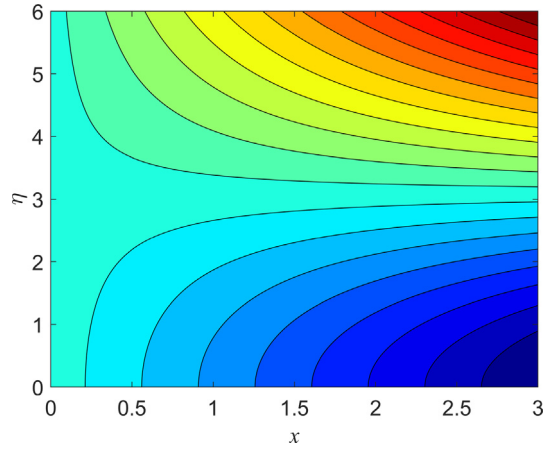

Fig. 23 The patterns of streamlines in the case of injection when $n = 0.5, M = 0.5, \tau = 0.5, \alpha = 0.1, m = 1$.

4. Final remarks

In the current paper, the impact of thermophoresis deposition on the flow of Sutterby nanofluid through a wedge geometry was examined. An efficient technique namely bvp4c is employed to obtain the numerical results of ODEs. The impacts of pertinent parameters on the flow field with mass and heat transport characteristics were examined. From this research, the following significant points are extracted.

- The velocity field augments have enhancing nature for the greater magnetic number in both SUC and INJ, while the temperature and concentration profiles and its relevant thickness of boundary-layer have decreasing nature.
- Due to the wedge parameter, the fluid velocity upsurges, whereas the concentration declines in both suction and injection. On the contrary, the temperature distribution augments in suction and declines in injection.
- The non-Newtonian parameter accelerates the fluid velocity in both cases.
- The friction factor and the Sherwood number in both cases decline due to the non-Newtonian parameter, while the Nusselt number augments.
- The thermophoretic and Brownian motion parameters upsurge the temperature of the fluid in both cases, whereas the concentration uplifts due to thermophoretic and declines due to Brownian motion.
- The relaxation parameter enhances the concentration and temperature in the case of SUC and declines in the case of INJ.
- The concentration of nanoparticle shrinks due to the thermophoresis factor and Schmidt number in both cases.
- The Nusselt number declines due to *Nb* and *Nt*.
- Due to *Nb*, the increasing rate of the concentration in the suction is 74.36%, whereas the decreasing rate in the injection is 11.93%.
- Due to *Nt*, the concentration rate is decelerated in the suction by 88.649%, while accelerated with the rate of 17.73% in the injection.

Declaration of competing interest

The authors affirm that they have no known competing financial interests or personal relationships that could have appeared to influence the scientific work reported in this paper.

Acknowledgements

The authors express their affectionate thanks to the respected Editor in chief and honorable reviewers for their valuable suggestions and comments to improve the presentation of this article.

References

[1] C. Cattaneo, Sulla Conduzione del Calore, Atti Sem. Mat. Fis. Univ. Modena. 3 (1948) 83–101.
[2] C.I. Christov, On frame indifferent formulation of the Maxwell-Cattaneo model of finite-speed heat conduction, Mech. Res. Commun. 36 (2009) 481–486, https://doi.org/10.1016/j.mechrescom.2008.11.003.
[3] J.V.R. Reddy, V. Sugunamma, N. Sandeep, Cross diffusion effects on MHD flow over three different geometries with Cattaneo-Christov heat flux, J. Mol. Liq. 223 (2016) 1234–1241, https://doi.org/10.1016/j.molliq.2016.09.047.
[4] A. Naseem, A. Shafiq, L. Zhao, M.U. Farooq, Analytical investigation of third grade nanofluidic flow over a riga plate using Cattaneo-Christov model, Results Phys. 9 (2018) 961–969, https://doi.org/10.1016/j.rinp.2018.01.013.
[5] A. Shafiq, S. Jabeen, T. Hayat, A. Alsaedi, Cattaneo-Christov heat flux model for squeezed flow of third grade fluid, Surf. Rev. Lett. 24 (2017) 1750098, https://doi.org/10.1142/S0218625X17500986.
[6] K. Hiemenz, Die Grenzschicht an einem in den gleichformigen Flussigkeitsstrom eingetauchten geraden Kreiszylinder, Dinglers Polytech. J. 326 (1911) 321–324.
[7] T.R. Mahapatra, A.S. Gupta, Heat transfer in stagnation-point flow towards a stretching sheet, Heat Mass Transf. 38 (2002) 517–521, https://doi.org/10.1007/s002310100215.
[8] R.U. Haq, S. Nadeem, Z. Hayat Khan, N. Sher Akbar, Thermal radiation and slip effects on MHD stagnation point flow of nanofluid over a stretching sheet, Phys. E Low-Dimensional

Syst. Nanostructures. 65 (2015) 17–23, https://doi.org/10.1016/j.physe.2014.07.013.
[9] A. Shafiq, Z. Hammouch, A. Turab, Impact of radiation in a stagnation point flow of Walters' B fluid towards a Riga plate, Therm. Sci. Eng. Prog. 6 (2018) 27–33, https://doi.org/10.1016/j.tsep.2017.11.005.
[10] U. Khan, A. Shafiq, A. Zaib, D. Baleanu, Hybrid nanofluid on mixed convective radiative flow from an irregular variably thick moving surface with convex and concave effects, Case Stud. Therm. Eng. 21 (2020) 100660, https://doi.org/10.1016/j.csite.2020.100660.
[11] F. Mabood, I. Tlili, A. Shafiq, Features of inclined magnetohydrodynamics on a second-grade fluid impinging on vertical stretching cylinder with suction and Newtonian heating, Math. Methods Appl. Sci. (2020) 1–13, https://doi.org/10.1002/mma.6489.
[12] X.-Y. Tian, B.-W. Li, Z.-M. Hu, Convective stagnation point flow of a MHD non-Newtonian nanofluid towards a stretching plate, Int. J. Heat Mass Transf. 127 (2018) 768–780, https://doi.org/10.1016/j.ijheatmasstransfer.2018.07.033.
[13] S.R. Mishra, I. Khan, Q.M. Al-mdallal, T. Asifa, Free convective micropolar fluid flow and heat transfer over a shrinking sheet with heat source, Case Stud. Therm. Eng. 11 (2018) 113–119, https://doi.org/10.1016/j.csite.2018.01.005.
[14] N.S. Ismail, N.M. Arifin, R. Nazar, N. Bachok, Stability analysis of unsteady MHD stagnation point flow and heat transfer over a shrinking sheet in the presence of viscous dissipation, Chinese J. Phys. 57 (2019) 116–126, https://doi.org/10.1016/j.cjph.2018.12.005.
[15] F.A. Soomro, R.U. Haq, Q.M. Al-Mdallal, Q. Zhang, Heat generation/absorption and nonlinear radiation effects on stagnation point flow of nanofluid along a moving surface, Results Phys. 8 (2018) 404–414, https://doi.org/10.1016/j.rinp.2017.12.037.
[16] M. Ijaz Khan, T. Hayat, F. Shah, F. Haq Mujeeb-Ur-Rahman, Physical aspects of CNTs and induced magnetic flux in stagnation point flow with quartic chemical reaction, Int. J. Heat Mass Transf. 135 (2019) 561–568, https://doi.org/10.1016/j.ijheatmasstransfer.2019.01.141.
[17] A. Shafiq, M.M. Rashidi, Z. Hammouch, I. Khan, Analytical investigation of stagnation point flow of Williamson liquid with melting phenomenon, Phys. Scr. 94 (2019) 35204, https://doi.org/10.1088/1402-4896/aaf548.
[18] A. Wakif, A novel numerical procedure for simulating steady MHD convective flows of radiative Casson fluids over a horizontal stretching sheet with irregular geometry under the combined influence of temperature-dependent viscosity and thermal conductivity, Math. Probl. Eng. 2020 (2020) Article ID 1675350, 20 pages. doi:10.1155/2020/1675350.
[19] M. Epstein, G.M. Hauser, R.E. Henry, Thermophoretic deposition of particles in natural convection flow from a vertical plate, J. Heat Transfer 107 (1985) 272–276, https://doi.org/10.1115/1.3247410.
[20] S.L. Goren, Thermophoresis of aerosol particles in the laminar boundary layer on a flat plate, J. Colloid Interface Sci. 61 (1977) 77–85, https://doi.org/10.1016/0021-9797(77)90416-7.
[21] S. Jayaraj, K.K. Dinesh, K.L. Pillai, Thermophoresis in natural convection with variable properties, Heat Mass Transf. 34 (1999) 469–475, https://doi.org/10.1007/s002310050284.
[22] A. Selim, M.A. Hossain, D.A.S. Rees, The effect of surface mass transfer on mixed convection flow past a heated vertical flat permeable plate with thermophoresis, Int. J. Therm. Sci. 42 (2003) 973–982, https://doi.org/10.1016/S1290-0729(03)00075-9.
[23] C.-C. Wang, Combined effects of inertia and thermophoresis on particle deposition onto a wafer with wavy surface, Int. J. Heat Mass Transf. 49 (2006) 1395–1402, https://doi.org/10.1016/j.ijheatmasstransfer.2005.09.036.
[24] A.J. Chamkha, I. Pop, Effect of thermophoresis particle deposition in free convection boundary layer from a vertical flat plate embedded in a porous medium, Int. Commun. Heat Mass Transf. 31 (2004) 421–430, https://doi.org/10.1016/j.icheatmasstransfer.2004.02.012.
[25] A. Postelnicu, Effects of thermophoresis particle deposition in free convection boundary layer from a horizontal flat plate embedded in a porous medium, Int. J. Heat Mass Transf. 50 (2007) 2981–2985, https://doi.org/10.1016/j.ijheatmasstransfer.2006.12.012.
[26] I. Muhaimin, R. Kandasamy, I. Hashim, Thermophoresis and chemical reaction effects on non-Darcy MHD mixed convective heat and mass transfer past a porous wedge in the presence of variable stream condition, Chem. Eng. Res. Des. 87 (2009) 1527–1535, https://doi.org/10.1016/j.cherd.2009.04.005.
[27] I.L. Animasaun, R.O. Ibraheem, B. Mahanthesh, H.A. Babatunde, A meta-analysis on the effects of haphazard motion of tiny/nano-sized particles on the dynamics and other physical properties of some fluids, Chinese J. Phys. 60 (2019) 676–687, https://doi.org/10.1016/j.cjph.2019.06.007.
[28] A. Wakif, I.L. Animasaun, P.V. Satya Narayana, G. Sarojamma, Meta-analysis on thermo-migration of tiny/nano-sized particles in the motion of various fluids, Chinese, J. Phys. (2019), https://doi.org/10.1016/j.cjph.2019.12.002.
[29] A. Zaib, S. Shafie, Slip Effect on an Unsteady MHD Stagnation-Point Flow of a Micropolar Fluid towards a Shrinking Sheet with Thermophoresis Effect, Int. J. Comput. Methods Eng. Sci. Mech. 16 (2015) 285–291, https://doi.org/10.1080/15502287.2015.1080317.
[30] S. Jain, R. Choudhary, Soret and dufour effects on thermophoretic MHD flow and heat transfer over a non-linear stretching sheet with chemical reaction, Int. J. Appl. Comput. Math. 4 (2018) 50, https://doi.org/10.1007/s40819-018-0481-2.
[31] J. Buongiorno, Convective transport in nanofluids, J. Heat Transfer 128 (2006) 240–250, https://doi.org/10.1115/1.2150834.
[32] A.V. Kuznetsov, D.A. Nield, The cheng-minkowycz problem for natural convective boundary layer flow in a porous medium saturated by a nanofluid: A revised model, Int. J. Heat Mass Transf. 65 (2013) 682–685, https://doi.org/10.1016/j.ijheatmasstransfer.2013.06.054.
[33] M.J. Uddin, M.N. Kabir, O.A. Bég, Computational investigation of Stefan blowing and multiple-slip effects on buoyancy-driven bioconvection nanofluid flow with microorganisms, Int. J. Heat Mass Transf. 95 (2016) 116–130, https://doi.org/10.1016/j.ijheatmasstransfer.2015.11.015.
[34] A. Wakif, A. Chamkha, T. Thumma, I.L. Animasaun, R. Sehaqui, Thermal radiation and surface roughness effects on the thermo-magneto-hydrodynamic stability of alumina-copper oxide hybrid nanofluids utilizing the generalized Buongiorno's nanofluid model, J. Therm. Anal. Calorim. (2020), https://doi.org/10.1007/s10973-020-09488-z.
[35] M. Zaydan, A. Wakif, I.L. Animasaun, U. Khan, D. Baleanu, R. Sehaqui, Significances of Blowing and Suction Processes on the Occurrence of Thermo-Magneto-Convection Phenomenon in a Narrow Nanofluidic Medium: A Revised Buongiorno's Nanofluid Model, Case Stud, Therm. Eng. (2020) 100726, https://doi.org/10.1016/j.csite.2020.100726.
[36] M.M. Rashidi, S. Abelman, N.F. Mehr, Entropy generation in steady MHD flow due to a rotating porous disk in a nanofluid, Int. J. Heat Mass Transf. 62 (2013) 515–525, https://doi.org/10.1016/j.ijheatmasstransfer.2013.03.004.
[37] M. Sheikholeslami, S. Abelman, D.D. Ganji, Numerical simulation of MHD nanofluid flow and heat transfer considering viscous dissipation, Int. J. Heat Mass Transf. 79 (2014) 212–222, https://doi.org/10.1016/j.ijheatmasstransfer.2014.08.004.
[38] M. Khan, Hashim, A. Hafeez, A review on slip-flow and heat transfer performance of nanofluids from a permeable shrinking

surface with thermal radiation: Dual solutions, Chem. Eng. Sci. 173 (2017) 1–11. doi:10.1016/j.ces.2017.07.024.
[39] A. Zahid, N. Sohail, S. Salman, E. Rahmat, Numerical study of unsteady flow and heat transfer CNT-based MHD nanofluid with variable viscosity over a permeable shrinking surface, Int. J. Numer. Meth. Heat Fluid Flow 29 (2019) 4607–4623, https://doi.org/10.1108/HFF-04-2019-0346.
[40] M. Ramezanizadeh, M. Alhuyi Nazari, Modeling thermal conductivity of Ag/water nanofluid by applying a mathematical correlation and artificial neural network, Int. J. Low-Carbon Technol. 14 (2019) 468–474, https://doi.org/10.1093/ijlct/ctz030.
[41] P. Besthapu, R.U. Haq, S. Bandari, Q.M. Al-Mdallal, Thermal radiation and slip effects on MHD stagnation point flow of non-Newtonian nanofluid over a convective stretching surface, Neural Comput. Appl. 31 (2019) 207–217, https://doi.org/10.1007/s00521-017-2992-x.
[42] K.U. Rehman, I. Shahzadi, M.Y. Malik, Q.M. Al-Mdallal, M. Zahri, On heat transfer in the presence of nano-sized particles suspended in a magnetized rotatory flow field, Case Stud. Therm. Eng. 14 (2019) 100457, https://doi.org/10.1016/j.csite.2019.100457.
[43] S. Aman, Q.M. Al-Mdallal, SA-copper based Maxwell nanofluid flow with second order slip effect using fractional derivatives, AIP Conf. Proc. 2116 (2019) 30021, https://doi.org/10.1063/1.5114005.
[44] P. Ragupathi, A.K.A. Hakeem, Q.M. Al-Mdallal, B. Ganga, S. Saranya, Non-uniform heat source/sink effects on the three-dimensional flow of Fe3O4 /Al2O3 nanoparticles with different base fluids past a Riga plate, Case Stud. Therm. Eng. 15 (2019) 100521, https://doi.org/10.1016/j.csite.2019.100521.
[45] U. Khan, A. Zaib, Z. Shah, D. Baleanu, E.-S.M. Sherif, Impact of magnetic field on boundary-layer flow of Sisko liquid comprising nanomaterials migration through radially shrinking/stretching surface with zero mass flux, J. Mater. Res. Technol. 9 (2020) 3699–3709, https://doi.org/10.1016/j.jmrt.2020.01.107.
[46] M. Ghalandari, A. Maleki, A. Haghighi, M. Safdari Shadloo, M. Alhuyi Nazari, I. Tlili, Applications of nanofluids containing carbon nanotubes in solar energy systems: A review, J. Mol. Liq. 313 (2020) 113476, https://doi.org/10.1016/j.molliq.2020.113476.
[47] S. Saranya, Q.M. Al-Mdallal, Non-Newtonian ferrofluid flow over an unsteady contracting cylinder under the influence of aligned magnetic field, Case Stud. Therm. Eng. 21 (2020) 100679, https://doi.org/10.1016/j.csite.2020.100679.
[48] M. Qasim, M.I. Afridi, A. Wakif, T.N. Thoi, A. Hussanan, Second Law Analysis of Unsteady MHD Viscous Flow over a Horizontal Stretching Sheet Heated Non-Uniformly in the Presence of Ohmic Heating: Utilization of Gear-Generalized Differential Quadrature Method, Entropy. 21 (2019) 1–25, https://doi.org/10.3390/e21030240.
[49] M. Qasim, M.I. Afridi, A. Wakif, S. Saleem, Influence of Variable Transport Properties on Nonlinear Radioactive Jeffrey Fluid Flow Over a Disk: Utilization of Generalized Differential Quadrature Method, Arab. J. Sci. Eng. 44 (2019) 5987–5996, https://doi.org/10.1007/s13369-019-03804-y.
[50] A. Wakif, M. Qasim, M.I. Afridi, S. Saleem, M.M. Al-Qarni, Numerical Examination of the Entropic Energy Harvesting in a Magnetohydrodynamic Dissipative Flow of Stokes' Second Problem: Utilization of the Gear-Generalized Differential Quadrature Method, J. Non-Equilibrium Thermodyn. (2019) 1–19, https://doi.org/10.1515/jnet-2018-0099.
[51] M. Qasim, Z. Ali, A. Wakif, Z. Boulahia, Numerical simulation of MHD peristaltic flow with variable electrical conductivity and Joule dissipation using generalized differential quadrature method, Commun. Theor. Phys. 71 (2019) 509–518, https://doi.org/10.1088/0253-6102/71/5/509.
[52] M.I. Afridi, A. Wakif, M. Qasim, A. Hussanan, Irreversibility Analysis of Dissipative Fluid Flow Over A Curved Surface Stimulated by Variable Thermal Conductivity and Uniform Magnetic Field: Utilization of Generalized Differential Quadrature Method, Entropy. 20 (2018) 1–15, https://doi.org/10.3390/e20120943.
[53] T. Thumma, A. Wakif, I.L. Animasaun, Generalized differential quadrature analysis of unsteady three-dimensional MHD radiating dissipative Casson fluid conveying tiny particles, Heat Transf. 49 (2020) 2595–2626, https://doi.org/10.1002/htj.21736.
[54] A. Wakif, Z. Boulahia, F. Ali, M.R. Eid, R. Sehaqui, Numerical Analysis of the Unsteady Natural Convection MHD Couette Nanofluid Flow in the Presence of Thermal Radiation Using Single and Two-Phase Nanofluid Models for Cu-Water Nanofluids, Int. J. Appl. Comput. Math. 4 (2018) 81, https://doi.org/10.1007/s40819-018-0513-y.
[55] I.M. Afridi, M. Qasim, A. Wakif, A. Hussanan, Second Law Analysis of Dissipative Nanofluid Flow over a Curved Surface in the Presence of Lorentz Force: Utilization of the Chebyshev–Gauss–Lobatto Spectral Method, Nanomaterials. 9 (2019) 1–21, https://doi.org/10.3390/nano9020195.
[56] G. Rasool, A. Wakif, Numerical Spectral Examination of EMHD Mixed Convective Flow of Second Grade Nanofluid towards a Vertical Riga Plate Using an Advanced Version of the Revised Buongiorno's Nanofluid Model, J. Therm. Anal. Calorim. (2020), https://doi.org/10.1007/s10973-020-09865-8.
[57] A.T. Patera, A spectral element method for fluid dynamics: Laminar flow in a channel expansion, J. Comput. Phys. 54 (1984) 468–488, https://doi.org/10.1016/0021-9991(84)90128-1.
[58] I. Mahariq, M. Kuzuoğlu, I.H. Tarman, H. Kurt, Photonic Nanojet Analysis by Spectral Element Method, IEEE Photonics J. 6 (2014) 1–14, https://doi.org/10.1109/JPHOT.2014.2361615.
[59] I. Mahariq, H. Kurt, M. Kuzuoğlu, Questioning degree of accuracy offered by the spectral element method in computational electromagnetics, Appl. Comput. Electromagnet. Soc. J. 30 (2015) 698–705.
[60] I. Mahariq, A. Erciyas, A spectral element method for the solution of magnetostatic fields, Turkish J. Electr. Eng. Comput. Sci. 25 (2017) 2922–2932.
[61] I. Mahariq, On the application of the spectral element method in electromagnetic problems involving domain decomposition, Turkish J. Electr. Eng. Comput. Sci. 25 (2017) 1059–1069.
[62] V.S. Patil, N.S. Patil, M.G. Timol, A remark on similarity analysis of boundary layer equations of a class of non-Newtonian fluids, Int. J. Non Linear Mech. 71 (2015) 127–131, https://doi.org/10.1016/j.ijnonlinmec.2014.10.022.
[63] T. Hayat, S. Afzal, M.I. Khan, A. Alsaedi, Irreversibility aspects to flow of Sutterby fluid subject to nonlinear heat flux and Joule heating, Appl. Nanosci. 9 (2019) 1215–1226, https://doi.org/10.1007/s13204-019-01015-3.
[64] N.A. Saif-ur-Rehman, M.S. Mir, M. Alqarni, M.Y. Farooq, Malik, Analysis of heat generation/absorption in thermally stratified Sutterby fluid flow with Cattaneo-Christov theory, Microsyst. Technol. 25 (2019) 3365–3373, https://doi.org/10.1007/s00542-019-04522-z.
[65] N.S. Akbar, Biomathematical study of Sutterby fluid model for blood flow in stenosed arteries, Int. J. Biomath. 08 (2015) 1550075, https://doi.org/10.1142/S1793524515500758.
[66] K.A. Yih, Uniform suction/blowing effect on forced convection about a wedge: Uniform heat flux, Acta Mech. 128 (1998) 173–181, https://doi.org/10.1007/BF01251888.
[67] N.A. Yacob, A. Ishak, I. Pop, Falkner-Skan problem for a static or moving wedge in nanofluids, Int. J. Therm. Sci. 50 (2011) 133–139, https://doi.org/10.1016/j.ijthermalsci.2010.10.008.